Volume 1 | Number 1 | Jan 2013 | Pages 1–100

Nanoscale

www.rsc.org/nanoscale

ROYAL SOCIETY OF CHEMISTRY

This is an *Accepted Manuscript*, which has been through the Royal Society of Chemistry peer review process and has been accepted for publication.

Accepted Manuscripts are published online shortly after acceptance, before technical editing, formatting and proof reading. Using this free service, authors can make their results available to the community, in citable form, before we publish the edited article. We will replace this *Accepted Manuscript* with the edited and formatted *Advance Article* as soon as it is available.

You can find more information about *Accepted Manuscripts* in the **Information for Authors**.

Please note that technical editing may introduce minor changes to the text and/or graphics, which may alter content. The journal's standard **Terms & Conditions** and the **Ethical guidelines** still apply. In no event shall the Royal Society of Chemistry be held responsible for any errors or omissions in this *Accepted Manuscript* or any consequences arising from the use of any information it contains.

Investigation of Localized Surface Plasmon Effect from Au Nanoparticles in ZnO Nanorods for Enhancing Performance of Polymer Solar Cells

Yu-Che Ho,[a] Shao-Hsuan Kao[a], Hsin-Che Lee,[a] Sheng-Kai Chang,[a] Cheng-Che Lee,[a] and Ching-Fuh Lin[*a,b,c]

[a] *Graduate Institute of Photonics and Optoelectronics, National Taiwan University, No. 1, Sec. 4, Roosevelt Road, Taipei 10617, Taiwan, ROC.*

[b] *Graduate Institute of Electronics Engineering, National Taiwan University, No. 1, Sec. 4, Roosevelt Road, Taipei 10617, Taiwan, ROC.*

[c] *Department of Electrical Engineering, National Taiwan University, No. 1, Sec. 4, Roosevelt Road, Taipei 10617, Taiwan, ROC.*

[*]*Corresponding author. Address: Institute of Photonics and Optoelectronics, National Taiwan University, Taipei, 10617 Taiwan, Republic of China. Tel: +886-2-33663540; Fax: +886-2-23642603. E-mail address: cflin@cc.ee.ntu.edu.tw*

Abstract

The organic polymer solar cell is recognized as one of the most competitive technologies in the next generation. Here we combine Au nanoparticles and ZnO nanorods to improve the inverted-structure low-bandgap polymer solar cells through enhancing the absorption and efficiency of the devices. However, the experiment shows that the Au nanoparticles tend to aggregate in the solution, thus reducing the localized surface plasmon resonance (LSPR) effect. The cluster effect on the spectral range of enhancement in the absorption is investigated and the absorption characteristics of the LSPR receive proper modification through our experiment. With the reduced Au nanoparticle clusters, the experiment clearly verifies the LSPR effect in the devices. The proper combination of the Au nanoparticles and ZnO nanorods leads to the power conversion efficiency of the

PTB7:PC$_{71}$BM inverted organic solar cell reaching 8.04% after optimizing the processes conditions.

1. Introduction

Over the past few years, organic solar cells have been regarded as the most prospective source of green energy in the future by taking its advantages of flexibility and potential to achieve large-scale and low-cost manufacturing under the solution process. [1-3]. The efficiency and the life time of polymer organic cells are influenced by the absorptivity and stability of the device structure and material. The inverted-structure organic solar cell adopts high work function metal as the anode and avoids PEDOT:PPS on ITO.[4, 5] It helps reduce the negative effects to the structure and life time, thus enhancing the efficiency and stability of the device.[6-16] Cs$_2$CO$_3$ [17, 18], TiO$_x$ [19, 20], and ZnO [21, 22] are three kinds of electron extraction layer that have been published in the articles to modify ITO. The features of ZnO are that it has a wide energy gap, the capability to match with the energy level of the polymer active layer, and the potential to allow large-scale solution process.[23] In earlier articles, there were discussions about different processes for generating a ZnO layer.[24, 25] Also, the method of growing ZnO nanorods via a hydrothermal process was used for penetrating into the active layer to extract carriers so that it could improve the short mobility distance of the organic material carrier and insufficient absorption caused by the lack of thickness on the device.

To further enhance the device performance, we adopt localized surface plasmon resonance (LSPR) effect and apply it with the ZnO nanorod arrays in the inverted-structure organic cell. The metal nanoparticles, Au in this study, are blended into the organic active material. With the organic active material flowing into the spacing of the ZnO nanorod arrays, the 4 nm Au nanoparticles can exist in the spacing of the ZnO nanorods. Because the free vibration electron on metallic surfaces interacts with the photons from external

interference, plasmon oscillation occurs and begins to transport dilatational waves along the metallic surface.[26] Moreover, due to the uncertainty principle, the matching criteria of light energy and momentum are easy to meet after the space is localized. This brings out an obvious enhanced electromagnetic resonance effect from the near field of the nanoparticle surface, which is called localized surface plasmon resonance.[27] In other words, through the application of surface plasmon resonance, the additional absorption (in particular the wave band) of the organic active layer material is therefore increased. In past studies, it was confirmed that adding metallic nanoparticles onto polymer solar cells or establishing ordered metallic nanostructure were effective for boosting the light absorption and the potential of photocurrent, thereby enhancing the photoelectric conversion efficiency.[28-30] Currently, there are applications that employ metallic nanoparticle surface plasmon resonance onto the conventional structure of the device [31-36] , the tandem polymer solar cells [37, 38], and the devices with nanorod structures and metallic nanoparticle sputtered on.[39, 40]

For LSPR, the size of nanoparticles has to be smaller than a certain number, such as smaller than 25 nm, to effectively excite the LSPR.[41] In addition, the absorption spectrum due to LSPR depends on the size of metallic nanoparticles.[41-43] However, past studies using metallic nanoparticles for polymer solar cells have not clearly indicated that the size of the added metallic nanoparticles well matches the mechanism of LSPR.[34] Therefore, it was impossible to distinguish exactly if the enhancement was prompted by the LSPR or the scattering effect. The aggregation would alter the main mechanism of metallic nanoparticles from the LSPR effect to the common scattering effect.[43]

From the experiment, we discovered that once the process was not kept in a low temperature environment, the Au nanoparticles in the solution would bring about intense clustering and affect their absorption spectrum performance on the LSPR effect. After the clustering, Au nanoparticles had a tendency to act as an enlarged effective size, so a red shift

appeared on the absorption spectrum. However, the result didn't seem to be observed as the expected performance from the actual Au nanoparticles size. In fact, the red shift on the absorption-enhanced band gave the device worse absorption performance. As a result, we discuss in the following on the solution we devised. In order to get the best absorption performance of a device, we used the pretreatment of ultrasonic vibration to break apart the clustering of Au and obtain the feature of absorption spectrum that matched the LSPR effect of the correct Au nanoparticles size. From above, we also verified that it was the surface plasmon effect giving to the enhancement of absorption.

Through adjusting the morphology, concentration, and doping method of Au nanoparticles, we were able to excite the surface plasmon effect of metallic nanoparticles by evenly doping the appropriate small-sized Au nanoparticles into the organic active material. We then applied the optimized morphology of ZnO nanorods with a longer length. Because of more volume of the rod spacing for active material to fill in, the effective thickness for light absorption is increased. Also, the ZnO nanorods that were embedded into the active layer can serve as a carrier pathway and help the carrier transport. Furthermore, the nanorod morphology of ZnO provided an amelioration of increasing the interface contact between organic and inorganic materials. Therefore, the optimization increased the absorption of the organic active layer, enhanced the transport and collection of carriers, and improved the absorption of light.[44, 45] In order to achieve the best performance, the thickness of MoOx hole transport layer which could influence the short-circuit current and fill factor was fine-tuned.[45] As a result, under single junction configurations, the development of an inverted-structure organic cell was encouraged to pursue higher efficiency performance. By employing the doping of small-sized Au nanoparticles to induce the surface plasmon effect and embedding a ZnO nanorod array in the organic active material, the PTB7: $PC_{71}BM$ inverted organic solar cell system reached 8.04% photoelectric conversion efficiency.

2.   Experiment

The devices were fabricated in an inverted structure. The active layer PTB7/PC$_{71}$BM was sandwiched between MoOx (molybdenum oxide) and ZnO, with ITO and Ag employed as electrodes.

In order to embed a ZnO nanorod array in the organic active material, a seed layer coating process and a hydrothermal growth process were used. Firstly, the sol-gel ZnO seed layer was prepared by mixing zinc acetate dehydrate (Zn(CH3COO)¬22H2O Sigma-Aldrich, ≥99.0%) in 2-methoxyethanol (CH3OCH2CH2OH) (Alfa Aesar, 99%) and ethanolamine (NH2CH2CH2OH). Secondly, the sol-gel was spin-coated on the cleaned ITO-coated glass substrate to form a ZnO seed layer. Afterwards, the device was annealed at 200℃ for an hour in nitrogen. In the next step, to fabricate the ZnO nanorod array, a growth-promoting solution for the hydrothermal process was prepared with zinc nitrate, HMT, and DI water. The hydrothermal process was implemented at 90℃ for 80 minutes, with the device suspended in the solution upside down. As the hydrothermal process finished, the device with the well-grown ZnO nanorod array was cleaned by IPA and DI water.

Next, to prepare the active layer material, PTB7/PC71BM (with a weight ratio of 1:1.5) was dissolved in 1,2-dichlorobenzene/chlorobenzene mixed solvent (with a volume ratio of 1:1) with a 3% additive solvent of 1,8-Diiodooctane (DIO). In order to fabricate the solar cell devices with LSPR, 4 nm Au nanoparticles were then blended into the active layer material. Moreover, after Au nanoparticles were blended, ultrasonic vibration pretreatment with different period of time (from 0 to 60 minutes) was adopted to reduce the aggregation of Au nanoparticles. Then the active layer material was spin-coated on the surface of the ZnO nanorod array in the glove box. A subsequent post-treatment of 5 hours dried in the glove box was applied.

Lastly, after the active layer being implemented, the devices were fabricated with molybdenum oxide (MoOx) deposited using thermal evaporation as the hole-transport layer and silver (~250 nm) as the back contact through thermal evaporation in a 3×10^{-6} Torr vacuum. The current density-voltage (J-V) characteristics were measured with a Keithley 2400 source meter under solar irradiation, simulated by a SUN 2000 (Abet Technologies, Inc.). The solar illumination, generated by a Thermo Oriel 150 W solar simulator with AM 1.5G filters, was calibrated at the intensity of 100 mW/cm2 by a NREL certificated mono-crystalline silicon reference cell (PVM-236). The incident photon conversion efficiency (IPCE) was measured, using QE-R-3015 (Enli Technology Co., Ltd.). The lamp was calibrated using a mono-crystalline silicon reference cell provided by Newport Corporation.

3. Results and Discussion

In the inverted-structure polymer solar cell, it is not easy to keep the high FF and level of the absorption and the photocurrent solely through alternating the concentration and thickness of the active layer. Hence, by combining ZnO nanorods and the surface plasmon effect of Au nanoparticles, Au nanoparticles can enhance the absorption. Also, the generated carriers that have been separated by the additional exciton can transport through the channel provided by ZnO nanorods. In this way, it helps the absorption of the active layer and makes even more effective use of solar light. Besides, in the past studies, we have proven and also applied ZnO nanorods to enhance the efficiency of the inverted polymer solar cell. [46-52] As a result, the ZnO nanorods, which were 90 nm in average height, 27 nm in average spacing and 25 nm in diameter was used as the electron transport channel.[53] The SEM images of ZnO nanorods and the active layer are shown in Figure 1. The thickness of the active layer was 160 nm. The devices with Au particles shown in Figure 1 (c) and Figure 1(d) had been pretreated with ultrasonic vibration. From the SEM images, the 20 nm Au can be observed.

They appear as bright spots above the nanorods in the SEM image. However, the 4 nm Au particles embedded inside the active layer cannot be observed because they were too small.

We added Au nanoparticles into the active layer of the device, which was embedded with ZnO nanorods. The illustration of the device is shown in Figure 2(a), and the energy band diagram is showed in Figure 2(b). The size of Au nanoparticles is important. First, it has to be small enough to be embedded into the spacing among ZnO nanorods. Second, the size should well correspond to the absorption spectrum of PTB7/PC$_{71}$BM blend so that the LSPR can be induced to enhance the solar-cell performance. In order to make an effective arrangement of morphology of ZnO nanorods and Au nanoparticles, we inferred from Figure 1, SEM images of ZnO nanorods, that if the Au nanoparticles were not chosen in appropriate size, they would stick on the top of the ZnO nanorod array and cause difficulty on the permeating of the active layer material. Therefore, the 4nm Au nanoparticles were adopted to apply in the active layer for coordinating with the ZnO nanorod spacing, ranging from less than 10 nm to over 40 nm, although the average was 20-30 nm. The method was to observe how the different Au nanoparticle concentrations influenced the absorption and efficiency performance of the solar cell.

By adding different concentrations of Au nanoparticles, the increase of the device's absorption spectrum band and absorption amount can be seen in Figure 3. From the observation of the absorption spectrum, we knew that the surface plasmon resonance of Au nanoparticles contributed a considerable degree of absorption on the organic active layer. In addition, when the concentration increased, the spectrum showed the absorption values rose around the range from 550 nm to 700 nm. The characteristic peak was located at 610 nm. Due to the increase of the active layer absorption, the amount of carriers increased, and the JSC of the device therefore increased as well.

However, according to Figure 4, the optical analysis of 4 nm Au nanoparticles size from nanoComposix Company, the localized surface plasmon of a 4 nm particle should correspond to around 500 nm absorption band, theoretically speaking. In comparison with the absorption measurements in Figure 3, the red shift of the increased absorption area did not match the localized surface plasmon effect of this nanoparticle size. Yet, at the same time, the absorption band, which was contributed by a localized surface plasmon effect, would theoretically move toward higher wavelengths as the particle size increased.[30, 41] Therefore, we inferred that the use and the preservation of 4 nm Au nanoparticles would affect its dispersion. If the dispersion was in poor circumstances, then it would cause a cluster and show an absorption tendency that is similar to the large particle size.

Figure 5 shows the atomic force microscopy (AFM) phase image analysis of the cluster and distribution condition with Au nanoparticles in the active layer. For the scan range of 500 nm x 500 nm, we observed a lot of clusters that were composed of many small dots. From the AFM, some small dots are under 10 nm and the size of the clusters ranges from 50 to 100 nm. The above confirms the distribution of the nanoparticles in the active layer: because of the selection of solution, the preservation method, and the stirring, the nanoparticles were not ideally distributed evenly, but rather unevenly clustered into small pieces. This phenomenon was attributed to the condition that the colloidal solution of Au nanoparticles was in an imbalanced state of thermodynamics, so the ambient temperature was likely to have a drastic impact on the preservation of the colloidal solution of Au nanoparticles. However, when preparing the active layer, the nanoparticles must separate from the low temperature and light-protected environment. Furthermore, it needed to go over the heating and stirring process so that the high temperature at this point would induce cluster and precipitation of the nanoparticles in the solution.

To further confirm that the cluster of Au nanoparticles had an impact on the shifts of absorption-enhanced wave band, and to prove the device enhancement was led by a localized surface plasmon effect, the solution was therefore prepared ahead. The solution adopted pretreatment of ultrasonic vibration to break apart aggregation or precipitation of Au nanoparticles and to improve its homodispersion. In the experiment prior to spin coat, we ultrasonically treated the active layer solution that contained 0.20mg/mL Au nanoparticles from 0 to 60 minutes. The method precipitated the cluster of Au nanoparticles, so the actual distribution of nanoparticles gradually became ideal. After fabricating the device, the measurement of absorption spectrum is exhibited in Figure 6. The measurement of the device efficiency performance is shown in Table 1 and its J-V curve is displayed in Figure 7. According to the absorption spectrum, as the processing time of ultrasonic vibration was increased, the absorption spectrum between 450 nm and 570 nm began to enhance. In the meantime, the absorption-enhanced characteristics above 600 nm started to decline after the treatment. The decline could be obviously observed soon after 1 or 2 minutes of treatment. As the process time of ultrasonic treatment prolonged to 60 minutes, the characteristic peak of the surface plasmon effect came near to 510 nm. On the contrary, the wave band where the absorption enhanced before going through the ultrasonic pretreatment now shared the same characteristics with the device that didn't add Au nanoparticles. Due to the fact that the Au nanoparticles started improving their dispersibility all over again, it reduced the chances of the cluster of lager-sized metallic nanoparticles. As a result, the surface plasmon effect of 4 nm Au nanoparticles was enhanced at 510 nm.

Therefore, through adjusting different concentrations of Au nanoparticles and then going through an ultrasonic vibration pretreatment process for 60 minutes, the devices that have been fabricated accordingly showed their absorption spectrum in Figure 8. Compared with Figure 4, the enhanced peak of this spectrum shows good correspondence to the absorption

characteristic of the metallic surface plasmon effect. It also shows that once the concentration increases, the absorption near the 510 nm band also enhances. While the concentration increases, the peak in the absorption shows an enhancement but without significant shift. Because the nanoparticles are dispersed through ultrasonic vibration, the peaks for various concentrations all appear between 450 nm and 570 nm. On the other hand, the LSPR effect is enhanced when there are more Au nanoparticles, so the peak increases with the concentration. In brief, in this series of experiments, we found that the application and pretreatment of metallic nanoparticles have an impact on the performance of the device. Meanwhile, by comparing the characteristics of the absorption before and after the treatment, we verified that the surface plasmon effect of metallic nanoparticles played the leading role on the device's absorption enhancement. Table 1 demonstrates the device performance from different concentrations of Au nanoparticles. In comparison with the device without Au nanoparticles, the one with Au nanoparticles enhanced the Jsc due to the fact that the Au nanoparticle surface plasmon effect contributed to the absorption enhancement of the active layer. Furthermore, the Jsc kept climbing up as the concentration added up. It reached its peak at 0.20 mg/mL and declined at 0.40 mg/mL.

The trend change of fill factor (FF) was similar to Jsc, but FF with Au nanoparticles performed worse than the ones without. FF fell from 65.5% to 65.9% for 0 to 0.20 mg/ml of Au nanoparticles, but it declined to 61.2% at 0.40 mg/mL. The variations here were attributed to Rs and Rsh. The conducting power of Au nanoparticles was far better than conductive organic materials. By adding the right amount of Au nanoparticles, it could also provide a carrier transport shortcut. Therefore, the series resistance of the device dropped as the addition of Au nanoparticles increased. The figure declined from 3.0Ω without Au nanoparticles to 2.7Ω with 0.40mg/mL of Au nanoparticles.

The addition of Au nanoparticles helped conductivity, yet the electrical conductivity direction was hard to control. Therefore, the leakage of current became severe as the concentration of Au nanoparticles increased. The parallel resistance dropped from 593 Ω without Au nanoparticles to 328 Ω with 0.40 mg/mL of Au nanoparticles as the Au nanoparticles increased. To conclude the above, when the Au nanoparticles concentration was too intense, it generated too many false transport channels, resulting in the loss of carriers. This condition influenced the performance of FF, and the Voc also declined as the concentration increased. As the energy level of Au was set around -5.1~ -5.47 eV (there were slight differences depending on the stacking patterns), it affected the carrier's ability to separate the built-in electric field on the donor-acceptor material interface. The exceeding addition would damage the material energy match of donor and accepter and caused the decline of Voc. The figure dropped from 0.71 V without Au nanoparticles to 0.65 V with 0.40 mg/mL of Au nanoparticles. The changes of Jsc and FF were decided by the positive and negative sides of the enhancement of device absorption, energy match, and carrier transport. Therefore we tried to maintain the dominance of high absorption and reduce the negative effects of carrier transport. The device increased the effect of its conversion efficiency from 7.22% without Au nanoparticles to 7.55% with 0.20 mg/mL of Au nanoparticles.

Even so, in order to achieve the best performance of the device, the thickness of the MoOx hole transport layer required adjustment for strengthening the transporting effect. It is cited that the thinner the active layer, the more sensitive to the thickness of MoOx.[45] Also the main factor of the above influences lies upon the short-circuit current and fill factor. Therefore, we took the optimal factor acquired from above to generate the device with diverse thicknesses of MoOx. The parameter of devices is shown in Table 2, and the J-V curve of the device is shown in Figure 9. When using 4 nm MoOx, the external quantum efficiency of the device reached the maximum, as shown in Figure 10, the Jsc enhanced to the

16.9 mA/cm2, and FF achieved 65.6%. Thus, the best device performance efficiency reached 7.88%. Lastly, the longer ZnO nanorod array was even tried to combine with the Au nanoparticle surface plasmon effect. By replacing the original use of a 90 nm ZnO nanorod array with 200±10 nm ZnO nanorod array, the enhancement of Jsc brought out higher conversion efficiency results and achieved optimal PCE of 8.04%. The performance is shown in Table 3.

4. Conclusion

We employed the Au nanoparticles into the active layer of the device and embedded it with a ZnO nanorod array. By adjusting the concentration and the method of doping, we were able to conclude the optimal matching of Au nanoparticles and ZnO nanorod array. Furthermore, the device successfully improved the absorption through the effect of surface plasmon, which is excited by the Au nanoparticles. Also, by the pretreatment of ultrasonic vibration, we effectively reduced the clustering of Au nanoparticles and disturbed the gain band position in the absorption spectrum regarding the surface plasmon effect. From the above results, we confirm that the surface plasmon effect plays a significant role in the absorption of a device. Consequently, the efficiency performance was enhanced from 7.22% to 7.55% through the surface plasmon. Lastly, by optimizing the device through offering a suitable hole transporting layer and an optimal ZnO nanorod array, the polymer solar cell with Au nanoparticles and ZnO nanorod array eventually enhanced the efficiency performance to 8.04% under the single junction configurations.

Nanoscale Accepted Manuscript

Notes and references

1.   C. J. Brabec, *Solar Energy Materials and Solar Cells*, 2004, **83**, 273.
2.   F. C. Krebs, *Solar Energy Materials and Solar Cells*, 2009, **93**, 394.
3.   B. C. Thompson and J. M. J. Fréchet, *Angewandte Chemie International Edition*, 2008, **47**, 58.
4.   M. Jørgensen, K. Norrman and F. C. Krebs, *Solar Energy Materials and Solar Cells*, 2008, **92**, 686.
5.   E. Voroshazi, B. Verreet, T. Aernouts and P. Heremans, *Solar Energy Materials and Solar Cells*, 2011, **95**, 1303.
6.   L.-M. Chen, Z. Hong, G. Li and Y. Yang, *Advanced Materials*, 2009, **21**, 1434.
7.   S. K. Hau, H.-L. Yip, N. S. Baek, J. Zou, K. O'Malley and A. K.-Y. Jen, *Applied Physics Letters*, 2008, **92**, 253301.
8.   H. Jing-Shun, C. Chen-Yu and L. Ching-Fuh, *Electron Device Letters, IEEE*, 2010, **31**, 332.
9.   Y.-J. Kang, C. Su Kim, D. Sung You, S. Hoon Jung, K. Lim, D.-G. Kim, J.-K. Kim, S. Hyung Kim, Y.-R. Shin, S.-H. Kwon and J.-W. Kang, *Applied Physics Letters*, 2011, **99**, 073308.
10.   C. S. Kim, S. S. Lee, E. D. Gomez, J. B. Kim and Y.-L. Loo, *Applied Physics Letters*, 2009, **94**, 113302.
11.   H. Cheun, C. Fuentes-Hernandez, Y. Zhou, W. J. Potscavage, S.-J. Kim, J. Shim, A. Dindar and B. Kippelen, *The Journal of Physical Chemistry C*, 2010, **114**, 20713.
12.   H.-H. Liao, L.-M. Chen, Z. Xu, G. Li and Y. Yang, *Applied Physics Letters*, 2008, **92**, 173303.
13.   J.-S. Huang, C.-Y. Chou, M.-Y. Liu, K.-H. Tsai, W.-H. Lin and C.-F. Lin, *Organic Electronics*, 2009, **10**, 1060.
14.   M.-Y. Lin, C.-Y. Lee, S.-C. Shiu, I.-J. Wang, J.-Y. Sun, W.-H. Wu, Y.-H. Lin, J.-S. Huang and C.-F. Lin, *Organic Electronics*, 2010, **11**, 1828.
15.   P.-C. Yang, J.-Y. Sun, S.-Y. Ma, Y.-M. Shen, Y.-H. Lin, C.-P. Chen and C.-F. Lin, *Solar Energy Materials and Solar Cells*, 2012, **98**, 351.
16.   V. Shrotriya, G. Li, Y. Yao, C.-W. Chu and Y. Yang, *Applied Physics Letters*, 2006, **88**, 073508.

17. Z. Xu, L.-M. Chen, G. Yang, C.-H. Huang, J. Hou, Y. Wu, G. Li, C.-S. Hsu and Y. Yang, 2009, **19**, 1227.

18. H.-H. Liao, L.-M. Chen, Z. Xu, G. Li and Y. Yang, *Applied Physics Letters*, 2008, **92**, 173303.

19. C. Waldauf, M. Morana, P. Denk, P. Schilinsky, K. Coakley, S. A. Choulis and C. J. Brabec, *Applied Physics Letters*, 2006, **89**, 233517.

20. Y.-J. Cheng, F.-Y. Cao, W.-C. Lin, C.-H. Chen and C.-H. Hsieh, *Chemistry of Materials*, 2011, **23**, 1512.

21. F. C. Krebs, S. A. Gevorgyan and J. Alstrup, *Journal of Materials Chemistry*, 2009, **19**, 5442.

22. H.-L. Yip, S. K. Hau, N. S. Baek, H. Ma and A. K. Y. Jen, *Advanced Materials*, 2008, **20**, 2376.

23. F. C. Krebs, M. Jørgensen, K. Norrman, O. Hagemann, J. Alstrup, T. D. Nielsen, J. Fyenbo, K. Larsen and J. Kristensen, *Solar Energy Materials and Solar Cells*, 2009, **93**, 422.

24. A. K. K. Kyaw, X. W. Sun, C. Y. Jiang, G. Q. Lo, D. W. Zhao and D. L. Kwong, *Applied Physics Letters*, 2008, **93**, 221107.

25. Y. Sun, J. H. Seo, C. J. Takacs, J. Seifter and A. J. Heeger, *Advanced Materials*, 2011, **23**, 1679.

26. W. L. Barnes, A. Dereux and T. W. Ebbesen, *Nature*, 2003, **424**, 824.

27. J. R. Sambles, G. W. Bradbery and F. Yang, *Contemporary Physics*, 1991, **32**, 173.

28. V. E. Ferry, J. N. Munday and H. A. Atwater, 2010, **22**, 4794.

29. Q. Gan, F. J. Bartoli and Z. H. Kafafi, 2013, **25**, 2385.

30. J. R. Cole and N. J. Halas, *Applied Physics Letters*, 2006, **89**, 153120.

31. J. Yang, J. You, C.-C. Chen, W.-C. Hsu, H.-r. Tan, X. W. Zhang, Z. Hong and Y. Yang, *ACS Nano*, 2011, **5**, 6210.

32. L. Qiao, D. Wang, L. Zuo, Y. Ye, J. Qian, H. Chen and S. He, *Applied Energy*, 2011, **88**, 848.

33. A. A. Harry and P. Albert, *Nature Materials*, 2010, **9**, 205.

34. J. Lee, Hwang, J. Park, Hwan, J. Kim, Soo, D. Lee, Yun and K. Cho, *Organic Electronics*, 2009, **10**, 416.

35. A. J. Morfa, K. L. Rowlen, T. H. Reilly, M. J. Romero and J. van de Lagemaat, *Applied Physics Letters*, 2008, **92**, 013504.

36. S.-S. Kim, S.-I. Na, J. Jo, D.-Y. Kim and Y.-C. Nah, *Applied Physics Letters*, 2008, **93**, 073307.

37. L. Lu, Z. Luo, T. Xu and L. Yu, *Nano Letters*, 2012, **13**, 59.

38. B. P. Rand, P. Peumans and S. R. Forrest, *Journal of Applied Physics*, 2004, **96**, 7519.

39. C. W. Cheng, E. J. Sie, B. Liu, C. H. A. Huan, T. C. Sum, H. D. Sun and H. J. Fan, *Applied Physics Letters*, 2010, **96**, 071107.

40. T. Singh, D. K. Pandya and R. Singh, *Thin Solid Films*, 2012, **520**, 4646.

41. S. Link and M. A. El-Sayed, *The Journal of Physical Chemistry B*, 1999, **103**, 8410.

42. S. Link and M. A. El-Sayed, *International Reviews In Physical Chemistry*, 1999, **19**, 409.

43. S. Link and M. A. El-Sayed, *The Journal of Physical Chemistry B*, 1999, **103**, 4212.

44. E. Galoppini, J. Rochford, H. Chen, G. Saraf, Y. Lu, A. Hagfeldt and G. Boschloo, *The Journal of Physical Chemistry B*, 2006, **110**, 16159.

45. Y.-H. Lin, P.-C. Yang, J.-S. Huang, G.-D. Huang, I.-J. Wang, W.-H. Wu, M.-Y. Lin, W.-F. Su and C.-F. Lin, *Solar Energy Materials and Solar Cells*, 2011, **95**, 2511.

46. N. Sekine, C.-H. Chou, W. L. Kwan and Y. Yang, *Organic Electronics*, 2009, **10**, 1473.

47. B. V. Andersson, A. Herland, S. Masich and O. Inganäs, *Nano Letters*, 2009, **9**, 853.

48. R. S. Singh, V. K. Rangari, S. Sanagapalli, V. Jayaraman, S. Mahendra and V. P. Singh, *Solar Energy Materials and Solar Cells*, 2004, **82**, 315.

49. L. Tsakalakos, J. Balch, J. Fronheiser, B. A. Korevaar, O. Sulima and J. Rand, *Applied Physics Letters*, 2007, **91**, 233117.

50. G. Conibeer, M. Green, R. Corkish, Y. Cho, E.-C. Cho, C.-W. Jiang, T. Fangsuwannarak, E. Pink, Y. Huang, T. Puzzer, T. Trupke, B. Richards, A. Shalav and K.-l. Lin, *Thin Solid Films*, 2006, **511–512**, 654.

51. V. Sivakov, G. Andrä, A. Gawlik, A. Berger, J. Plentz, F. Falk and S. H. Christiansen, *Nano Letters*, 2009, **9**, 1549.

52. P.-Y. Ho, S. Thiyagu, S.-H. Kao, C.-Y. Kao and C.-F. Lin, *Nanoscale*, 2014, **6**, 466.

53. S.-H. Kao, Z.-L. Tseng, P.-Y. Ho, C.-Y. Kao, S. Thiyagu and C.-F. Lin, *Journal of Materials Chemistry A*, 2013, **1**, 14641.

Figure Captions

Figure 1 The SEM top view (a) and front view (b) of a ZnO nanorod array; and the SEM front view of the active layer with 4 nm (c) and with both 4 nm and 20 nm (d) Au nanoparticles.

Figure 2 The structure illustration (a) and the energy band diagram (b) of the polymer solar cell with Au nanoparticles and ZnO nanorod array.

Figure 3 The comparison between the absorption spectra of organic active layer devices added, respectively, with 0.10 mg/mL, 0.15mg/mL, 0.20 mg/mL, 0.30 mg/mL, 0.40mg/mL Au nanoparticles, and without.

Figure 4 The optical absorption characteristic of the surface plasmon by 4nm Au nanoparticles. This spectrum is provided by nanoComposix Inc.

Figure 5 The AFM images of PTB7: $PC_{71}BM$ active layer surface which was added with 0.20 mg/mL Au nanoparticles.

Figure 6 The comparison between the absorption spectra of organic active layer devices added with and without Au nanoparticles 0.20 mg/mL via different periods of time of ultrasonic vibration pretreatment.

Figure 7 The current-voltage characteristic of the organic active layer devices added with and without Au nanoparticles 0.20 mg/mL via different periods of time of ultrasonic vibration pretreatment.

Figure 8 The comparison between the absorption spectra of organic active layer devices added, respectively, with 0.10 mg/mL, 0.15mg/mL, 0.20 mg/mL, 0.30 mg/mL, 0.40mg/mL Au nanoparticles, and without, by ultrasonic vibration pretreatment for an hour.

Figure 9 The current-voltage characteristic of the organic solar cells with Au nanoparticles with the evaporation thickness of MoOx hole transport layer is in adjustment.

Figure 10 The external quantum efficiency of the organic solar cells with Au nanoparticles with the evaporation thickness of MoOx hole transport layer is in adjustment.

Table Captions

Table 1 The performance of PTB7:PC$_{71}$BM organic solar cell using a ZnO nanorod array by adding different concentration of 4 nm Au nanoparticles.

Table 2 The influence on the device performance by adjusting diverse thicknesses of the MoOx hole transporting layer.

Table 3 The device performance of 4 nm Au nanoparticles combined with 200±10 nm ZnO nanorods.

Table 1

ZnO nanorod array:PTB7/PC$_{71}$BM	PCE (%)	Jsc (mA/cm^2)	Voc (V)	FF (%)	Rs (Ω/cm^2)	Rsh (Ω /cm^2)
w/o 4nm Au NPs	7.22	15.2	0.71	66.9	3.0	593
4nm Au NPs 0.10mg/mL	7.35	16.0	0.70	65.6	2.8	610
4nm Au NPs 0.15mg/mL	7.52	16.4	0.70	65.5	2.9	593
4nm Au NPs 0.20mg/mL	7.55	16.6	0.69	65.9	2.7	599
4nm Au NPs 0.30mg/mL	6.73	16.0	0.66	63.7	2.8	500
4nm Au NPs 0.40mg/mL	6.17	15.5	0.65	61.2	2.7	328

Table 2

ZnO nanorod array:PTB7/PC$_{71}$BM With Au NPs	PCE (%)	Jsc (mA/cm^2)	Voc (V)	FF (%)	Rs (Ω/cm^2)	Rsh (Ω /cm^2)
1 nm MoOx as HTL	6.25	14.6	0.71	60.3	3.9	401
2 nm MoOx as HTL	7.17	16.0	0.71	63.1	4.0	501
3 nm MoOx as HTL	7.74	16.8	0.71	64.9	4.0	544
4 nm MoOx as HTL	7.88	16.9	0.71	65.6	4.1	601
5 nm MoOx as HTL	7.54	16.3	0.71	65.1	4.5	596
6 nm MoOx as HTL	7.46	16.2	0.71	64.8	5.0	598

Table 3

ZnO nanorod array:PTB7/PC$_{71}$BM With Au NPs (Using ZnO nanorod length 200±10nm)	PCE (%)	Jsc (mA/cm^2)	Voc (V)	FF (%)	Rs (Ω/cm^2)	Rsh (Ω /cm^2)
	8.04	17.5	0.71	64.7	4.0	529
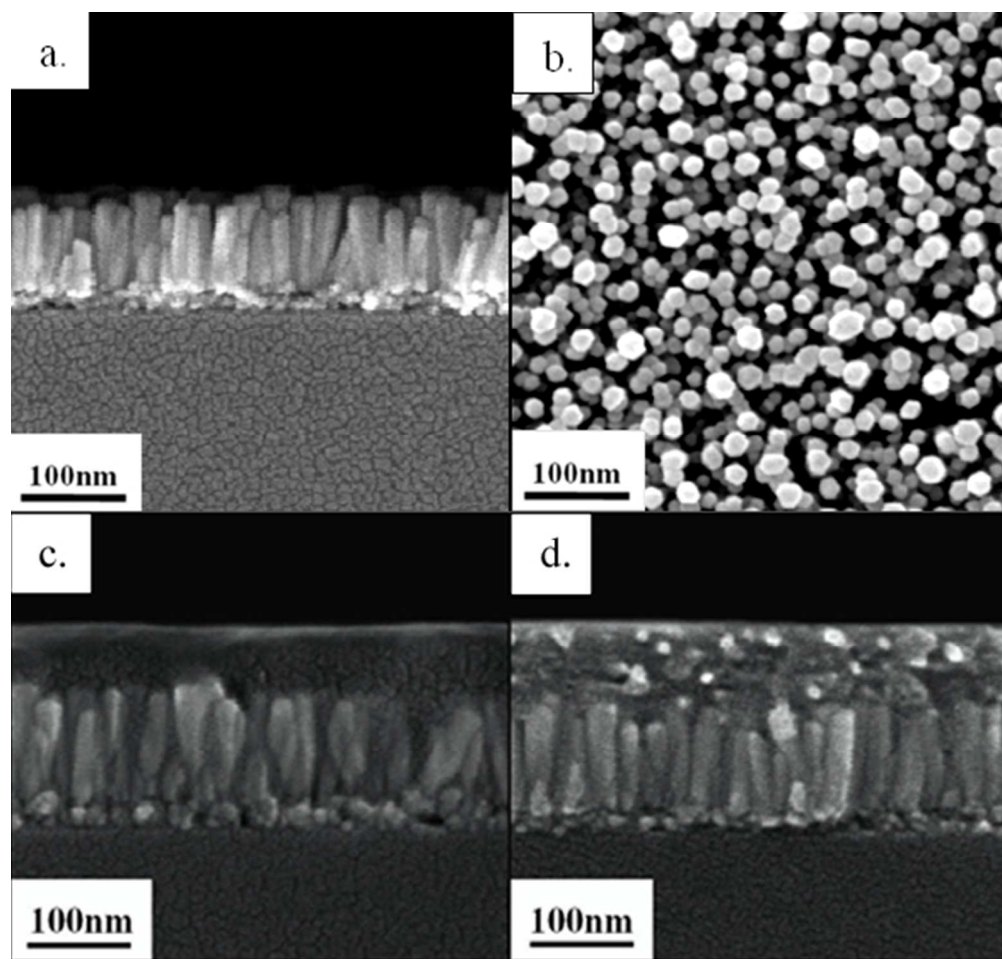
Figure 1 The SEM top view (a) and front view (b) of a ZnO nanorod array; and the SEM front view of the active layer with 4 nm (c) and with both 4 nm and 20 nm (d) Au nanoparticles.
99x94mm (150 x 150 DPI)
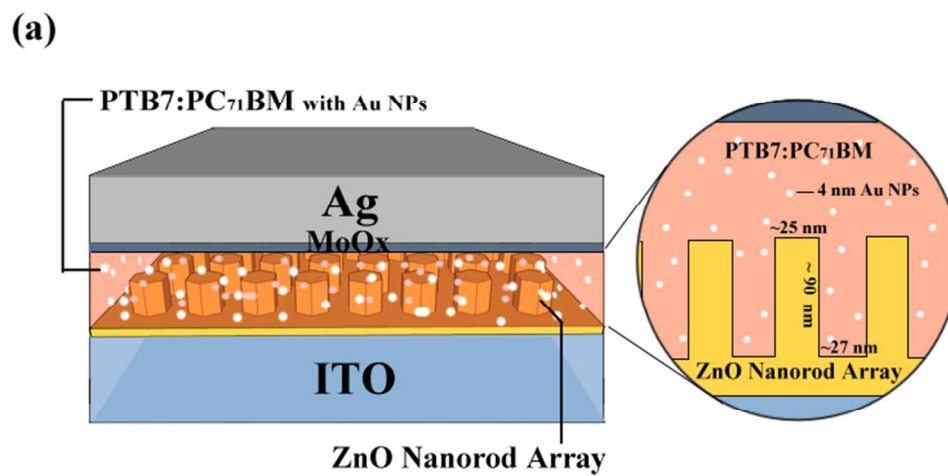
(a)

Figure 2 The structure illustration (a) and the energy band diagram (b) of the polymer solar cell with Au nanoparticles and ZnO nanorod array.
273x140mm (72 x 72 DPI)
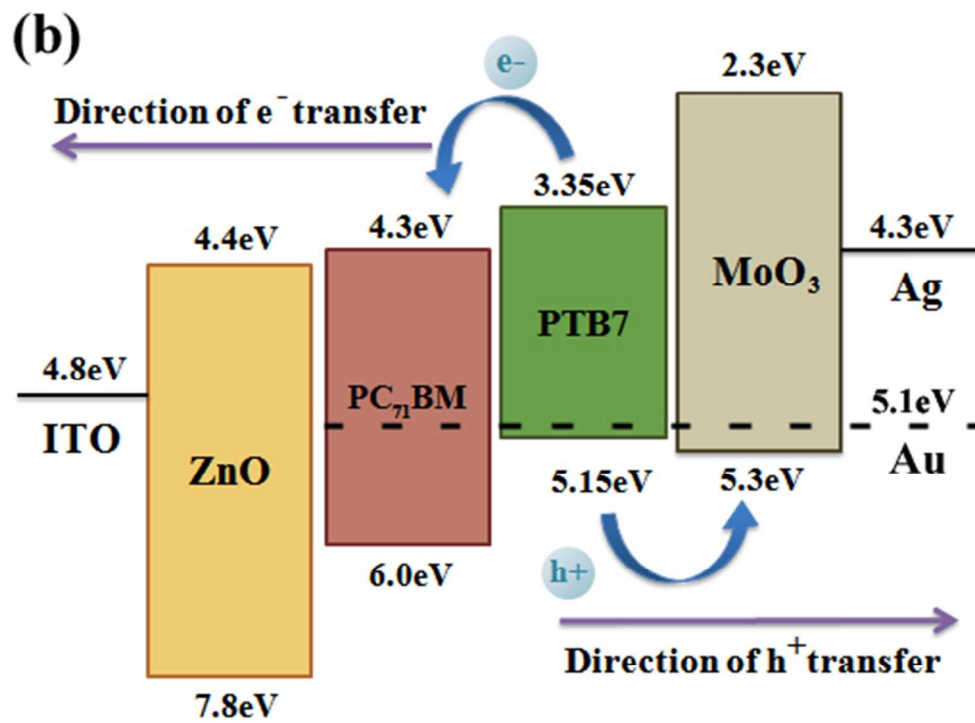
(b)

Figure 2 The structure illustration (a) and the energy band diagram (b) of the polymer solar cell with Au nanoparticles and ZnO nanorod array.
184x140mm (72 x 72 DPI)
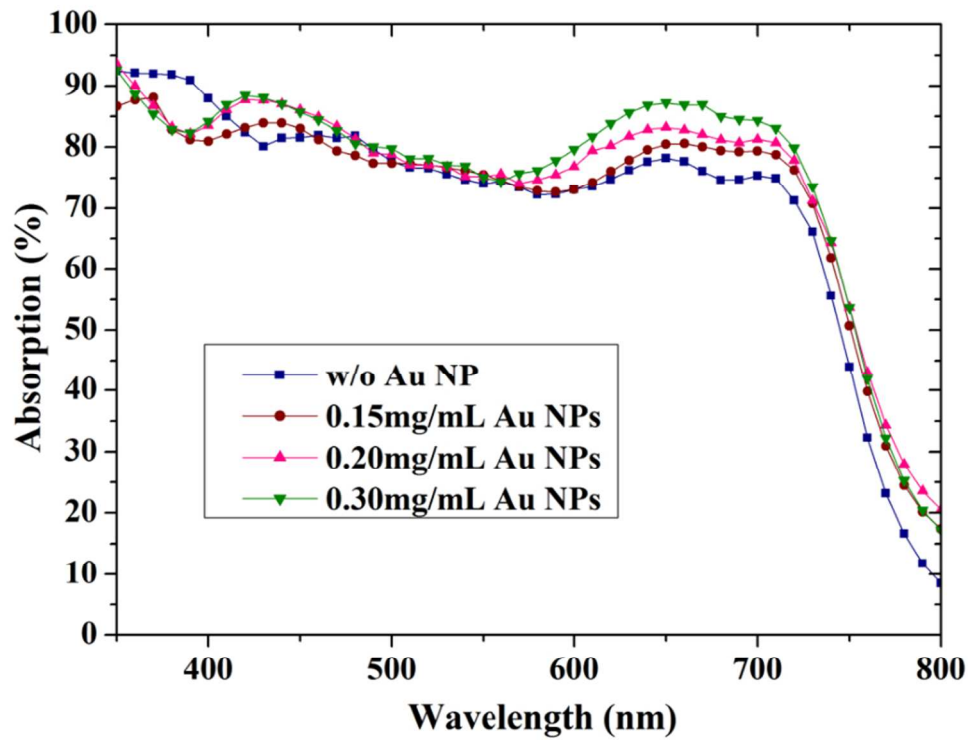
Figure 3 The comparison between the absorption spectra of organic active layer devices added, respectively, with 0.10 mg/mL, 0.15mg/mL, 0.20 mg/mL, 0.30 mg/mL, 0.40mg/mL Au nanoparticles, and without.
112x85mm (209 x 209 DPI)
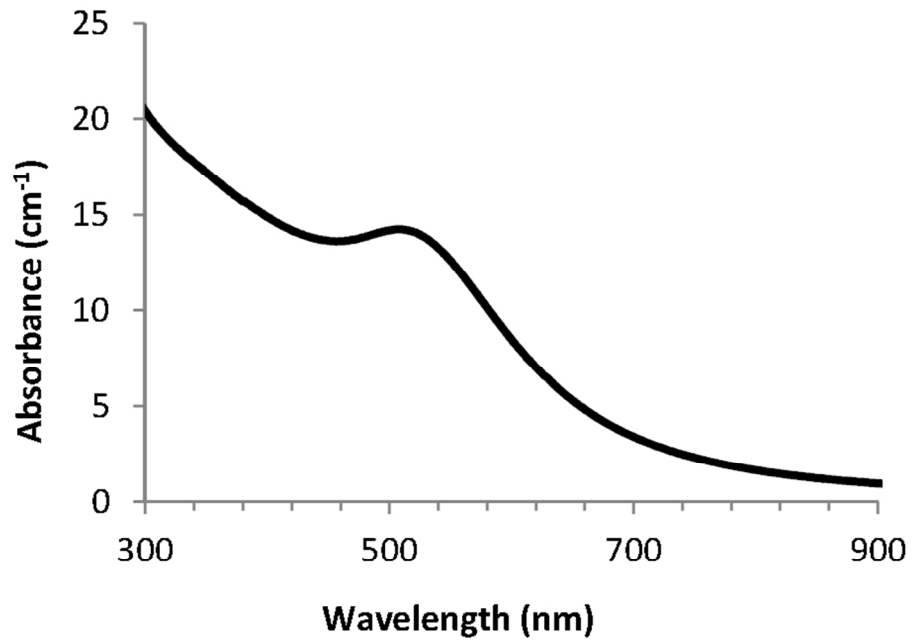
Figure 4 The optical absorption characteristic of the surface plasmon by 4nm Au nanoparticles. This spectrum is provided by nanoComposix Inc.
357x273mm (72 x 72 DPI)
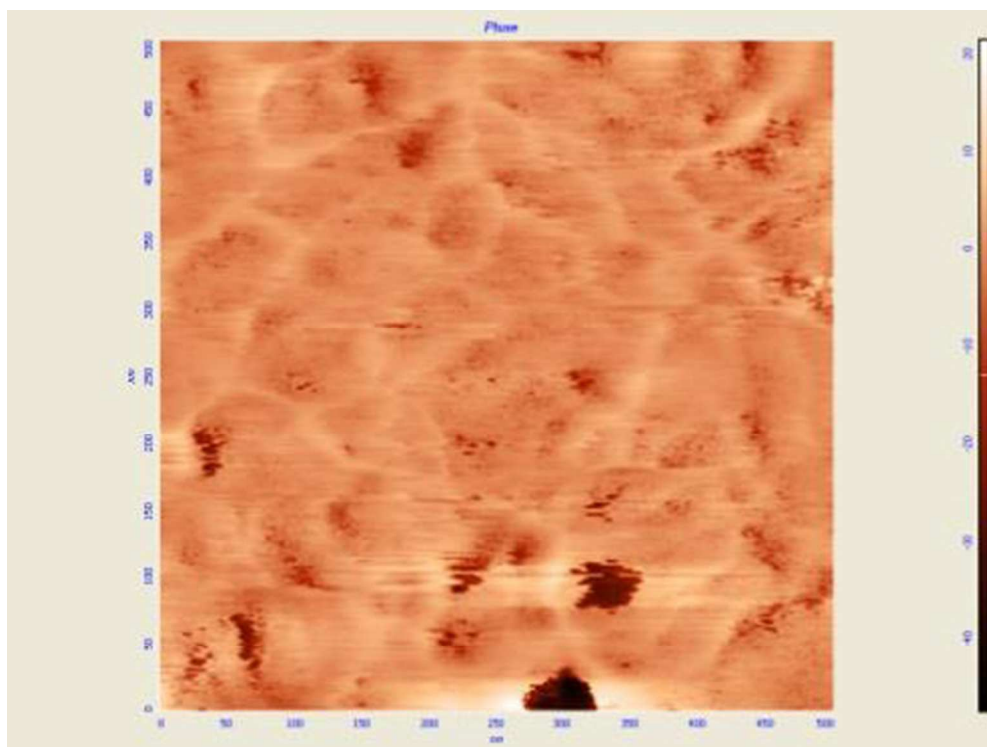
Figure 5 The AFM images of PTB7: PC71BM active layer surface which was added with 0.20 mg/mL Au
nanoparticles.
74x55mm (168 x 168 DPI)
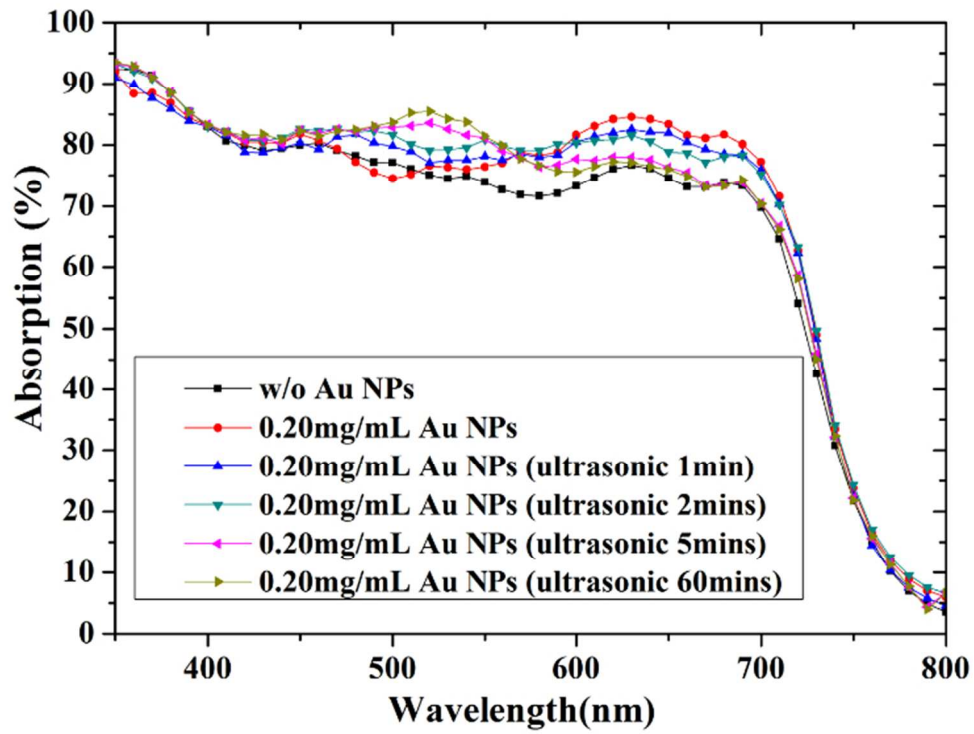
Figure 6 The comparison between the absorption spectra of organic active layer devices added with and without Au nanoparticles 0.20 mg/mL via different periods of time of ultrasonic vibration pretreatment. 120x90mm (161 x 161 DPI)
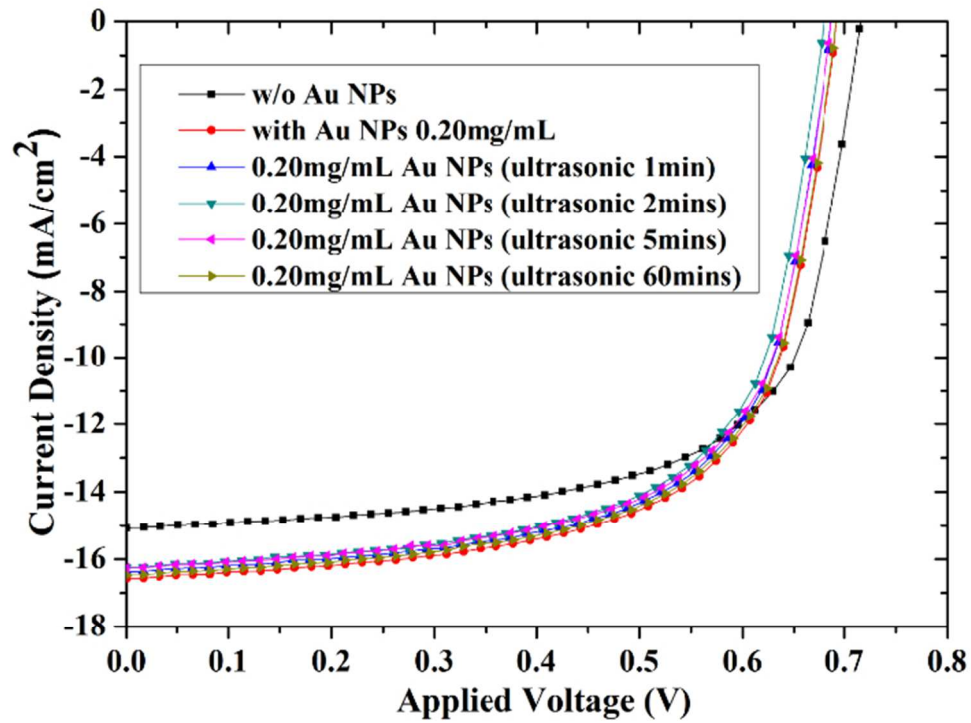
Figure 7 The current-voltage characteristic of the organic active layer devices added with and without Au nanoparticles 0.20 mg/mL via different periods of time of ultrasonic vibration pretreatment.
110x80mm (169 x 169 DPI)
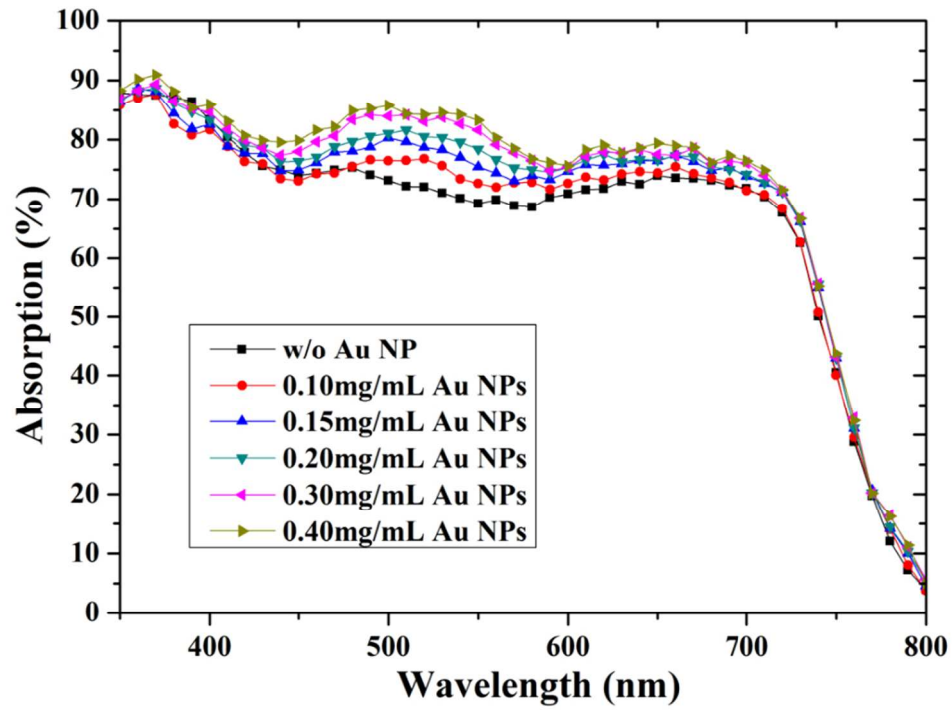
Figure 8 The comparison between the absorption spectra of organic active layer devices added, respectively, with 0.10 mg/mL, 0.15mg/mL, 0.20 mg/mL, 0.30 mg/mL, 0.40mg/mL Au nanoparticles, and without, by ultrasonic vibration pretreatment for an hour.
119x84mm (214 x 214 DPI)
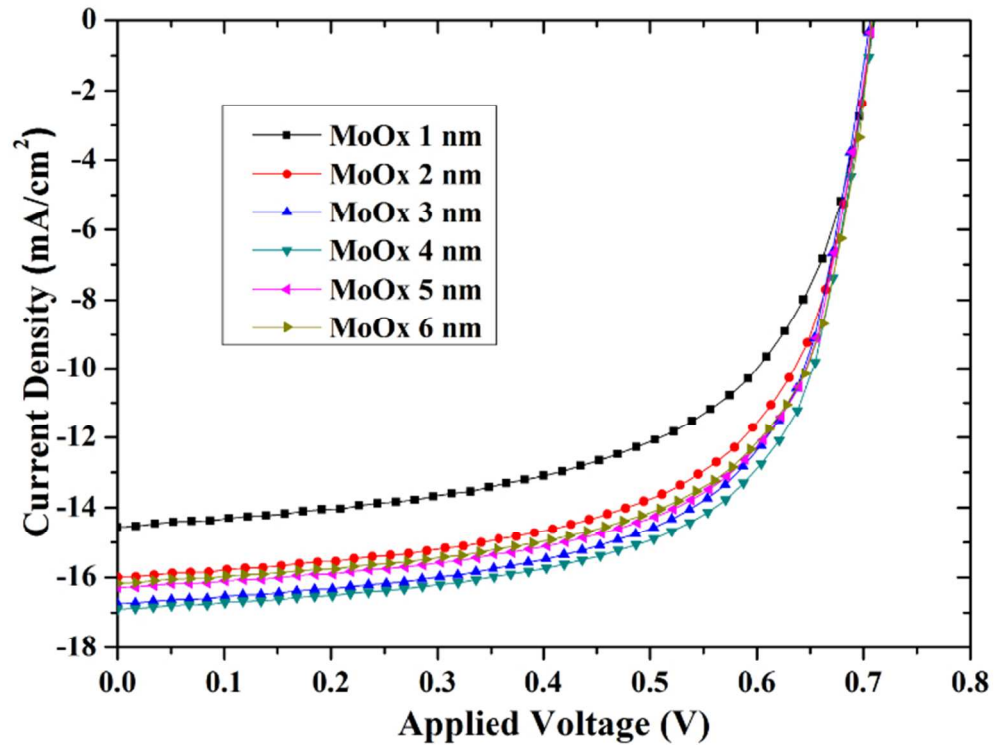
Figure 9 The current-voltage characteristic of the organic solar cells with Au nanoparticles with the evaporation thickness of MoOx hole transport layer is in adjustment.
115x85mm (170 x 170 DPI)
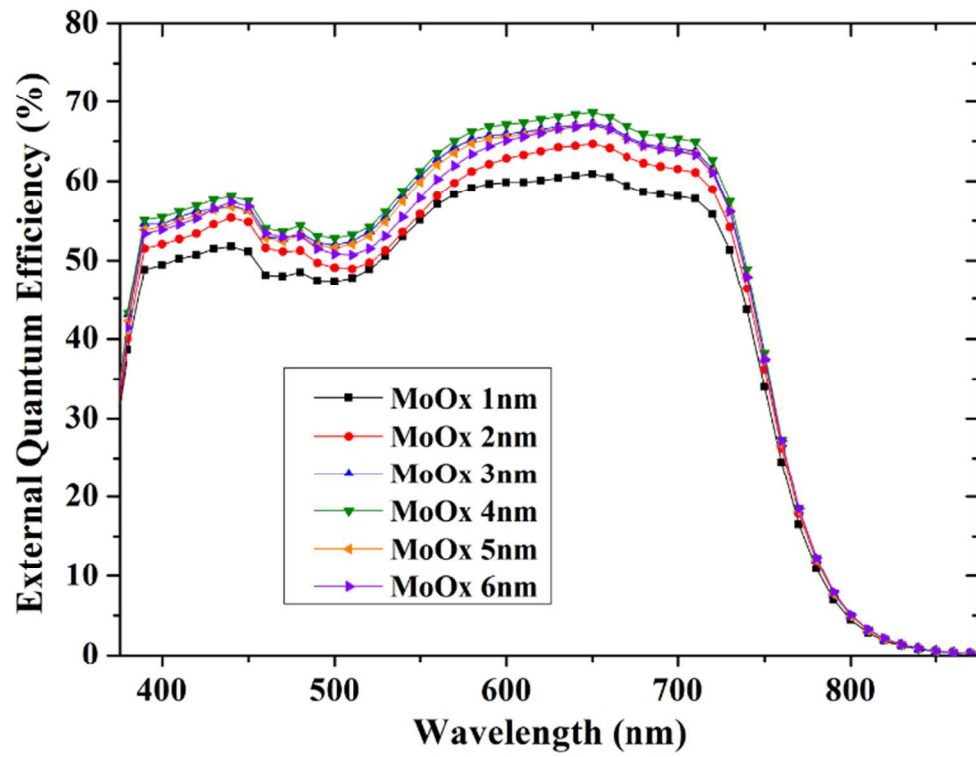
Figure 10　The external quantum efficiency of the organic solar cells with Au nanoparticles with the evaporation thickness of MoOx hole transport layer is in adjustment.
115x86mm (174 x 174 DPI)